American Mineralogist, Volume 87, pages 1121–1127, 2002

Structural relationships in $(Mn_{1-x}Zn_x)Mn_2O_4$ $(0 \le x \le 0.26)$: The "dragging effect" of the tetrahedron on the octahedron

FERDINANDO BOSI,[1,]* SERGIO LUCCHESI,[1] AND ANTONIO DELLA GIUSTA[2]

[1]Dipartimento di Scienze della Terra, Università di Roma "La Sapienza," P.le A.Moro 5, 00185 Roma, Italy
[2]Dipartimento di Mineralogia e Petrologia, Università di Padova, C.so G.Garibaldi 37, 35122 Padova, Italy

ABSTRACT

Ten hausmannite crystals (from Ilfeld and Friedrichrode, Harz, Germany), belonging to the $(Mn_{1-x}Zn_x)Mn_2O_4$ $(0 \le x \le 0.26)$ system ($I4_1/amd$ hausmannite structure type), were characterized by chemical (electron microprobe) and structural (single-crystal X-ray diffractometer) analysis. The prevailing trivalent cation is Mn^{3+}, with very minor Al (not higher than 0.005 apfu). Among divalent cations, the main substitution involves $Zn \rightarrow Mn^{2+}$. Cation distribution was obtained by comparing chemical and structural data, and results confirm normal distribution, with Mn^{3+} ordered on the octahedral site. A specific bond distance of 2.030 Å was refined for $^{VI}Mn^{3+}$-O.

Unit-cell parameters a and c range from 5.752 to 5.763 Å and from 9.408 to 9.461 Å, respectively. The smallest values are characteristic of the sample with the highest hetaerolite content. T-O bond distance (2.027–2.041 Å) shows a strong positive correlation with unit-cell constants, while the O-T-O angle (103.3–103.7°) is related only to the oxygen coordinate, z. The two octahedral bond distances show limited variations: the shorter one, M-O_S, ranges from 1.927 to 1.930 Å, and is not significantly correlated with unit-cell parameters. The longer one, M-O_L, shows a larger variation, from 2.281 to 2.290 Å, and is positively correlated with c. Regularization of the octahedron with increasing hetaerolite content coincides with an increase in the oxygen coordinate y and a decrease in c and c/a. Of particular interest is the positive linear relation between octahedral elongation and V_T. As the octahedral content of all samples is almost constant, given the closeness of Mn^{3+} to stoichiometry, all structural distortions are linked to $^{IV}Zn \rightarrow {}^{IV}Mn^{2+}$ that reduces the T-O bond distance and causes movement of the structure toward cubic symmetry. This interaction is due to the "dragging effect" of the tetrahedron on the octahedron.

In hausmannite-type structures, besides the main structural distortion produced by the Jahn-Teller effect, a secondary one, without symmetry modification, is determined by the geometrical effects of the tetrahedron on the octahedron.

INTRODUCTION

AB_2O_4 oxides may be described by the $^{IV}(A_{1-i}B_i)^{VI}(B_{2-i}A_i)O_4$ structural formula, in which IV and VI represent tetrahedrally and octahedrally coordinated sites, A and B are cations with variable valence, and i is the inversion parameter. Depending on the nature and electronic configuration of the coordinating cations, these sites may be more or less distorted. In particular, in the case of the spinel structure (Hafner 1960; Hill et al. 1979), $Fd\bar{3}m$ symmetry results from occupancy of the octahedral (M) and tetrahedral (T) sites, both with fixed coordinates but, whereas the tetrahedron is regular (point symmetry $\bar{4}3m$), the octahedron is distorted (point symmetry $\bar{3}m$). However, this distortion only involves the bond angles as all bond distances remain equivalent. The oxygen atom (point symmetry $\bar{3}m$) is defined by (u, u, u) coordinates, setting the origin at $\bar{3}m$. The cell parameter and oxygen coordinate are therefore functions of tetrahedral and octahedral bond distances (Hill et al. 1979).

Among A and B cations, the presence of transition elements with unpaired external electronic levels causes large distortions in both sites, due to the Jahn-Teller effect. In particular, cations with $3d^9$ or $3d^4$ orbitals such as Cu^{2+} and Mn^{3+}, when in octahedral coordination, produce lowering of site symmetry to that of a tetragonal bipyramid, due to the establishment of different interactions along the previously equivalent M-O bonds. In the presence of Mn^{3+}, the final results are two long bond distances, M-O_L, along the tetragonal axis of the bipyramid, and four shorter ones, M-O_S, in the basal plane. In cubic spinels, when $^{VI}Mn^{3+}$ is present in low concentrations, the octahedra are deformed. However, elongation does not produce macroscopic effects such as point symmetry modifications, because the distortions occur at random along the equivalent [100] directions. As soon as a critical $^{VI}Mn^{3+}$ concentration and critical temperature are reached (Golikov et al. 1989), mutual interactions between second-coordination spheres become important and all octahedra are deformed along the same direction, as in hausmannite ($MnMn_2O_4$). The general effect is a departure from cubic spinel $Fd\bar{3}m$ symmetry to tetragonal $I4_1/amd$ symmetry (Satomi 1961; Jarosch 1987), with the tetragonal c axis approximately parallel to M-O_L and the four M-O_S approximately

* E-mail: ferdinando.bosi@uniroma1.it

0003-004X/02/0809–1121$05.00

parallel to (001). Two O-M-O angles are necessary to describe the octahedron fully: O_S-M-O_S and O_S-M-O_L, and its symmetry is thus reduced to $2/m$, but site coordinates are still fixed. In this structure, the tetrahedra still show four equivalent T-O distances, but the O-T-O angle departs from ideality (109.47°). As a consequence, site point symmetry is lowered from that of a tetrahedron to a tetragonal bisphenoid ($\bar{4}2m$, with fixed coordinates). The distortion produces a further movement of the oxygen atom, which is now defined by two variable coordinates (0, y, z – point symmetry m). Structural parameters (a, c, y and z) and bond distances and angles are related by geometrical relations (see Appendix). These functions may be reduced to those describing $Fd\bar{3}m$ spinel geometry (Hill et al. 1979).

EXPERIMENTAL METHODS

The ten crystals that we examined were kindly made available by the "Museo di Mineralogia" of the University of Rome "La Sapienza" (Table 1). All crystals (from Ilfeld and Friedrichrode, Harz, Germany) are {111} specimens (from 0.1 to 2 mm), at times constituting {101} polysynthetic twins, associated with barite and, in the case of 6A, also with pyrolusite. Samples were crushed, and homogeneous, equidimensional, single crystals (100–200 μm) were handpicked and prepared for X-ray diffraction (XRD) analysis.

X-ray data collection was performed on a Siemens P4 automated four-circle single-crystal diffractometer according to the conditions listed in Table 2. One-eighth of the reciprocal space was examined for intensity collection. Scan speed varied, depending on reflection intensity, estimated with a pre-scan. Background was measured with a stationary counter and crystal at the beginning and end of each scan, in both cases for half the scan time. Three standard reflections were monitored every 47 measurements.

Data reduction and structure refinement were performed with the SHELXTL-PC program package furnished by Siemens Analytical X-ray Instruments, Inc. XRD intensities were initially corrected for polarization and Lorentz effects. An absorption correction was performed using a semi-empirical method. Reflections with $I > 2\sigma(I)$ were considered as observed. No significant deviations from $I4_1/amd$ symmetry were recorded. Initial atomic coordinates were taken from Jarosch (1987). The scale factor, oxygen coordinates, T and M occupancies, thermal factors, and isotropic secondary extinction coefficient were variable parameters. No chemical constraints were used during refinement. Fully ionized scattering curves for all elements were used except for O (80% ionized), because they furnished the best values of conventional agreement factors over all $\sin\theta/\lambda$ intervals. Three cycles of isotropic refinement were followed by anisotropic cycles until convergence. The R values were very satisfactory (Table 3). For the sake of brevity, only U_{eq} are listed in Table 3 (anisotropic displacement parameters may be obtained from the authors).

The same crystals used for X-ray data collection were mounted on glass slides and polished for electron microprobe analysis. The analyses were obtained by wavelength-dispersive methods using a Cameca-Camebax instrument. Operating conditions were 15KV accelerating potential and a sample current of 15nA, the PAP data reduction program was used (Table 4). Synthetic oxide standards (MgO, Fe_2O_3, ZnS, NiO, Al_2O_3, Cr_2O_3, $MnTiO_2$, wollastonite, vanadinite) were used. Each element determination was accepted after checking that I_{Xstd}/I_{std} (I = intensity of analyzed standard before I_{Xstd} and after I_{std} each determination) was within 1.00 ± 0.01. Precision for major elements (Mn, Zn) was usually within 1% of the actual amount present, and that of minor elements within 5%. Fe, Ni, Ti, Si, V, and Cr were considered not detected, because their measured amounts were below their uncertainties. Mn^{3+} was calculated on the basis of stoichiometry assuming 3 cations for 4 oxygen atoms.

TABLE 1. Source of hausmannite samples

Sample	Provenance	No.
2A	Friedrichrode, Germany	3339/2
2B	Friedrichrode, Germany	3339/2
3A	Friedrichrode, Germany	3340/3
3B	Friedrichrode, Germany	3340/3
4B	Friedrichrode, Germany	3341/4
4C	Friedrichrode, Germany	3341/4
5A	Friedrichrode, Germany	3342/5
6A	Friedrichrode, Germany	3343/6
8A	Ilfeld, Germany	3345/8
8B	Ilfeld, Germany	3345/8

TABLE 2. Parameters for X-ray data collection

Unit-cell parameter determination	
Radiation	Mo$K\alpha_1$ (0.70930 Å)
Reflections used	12 (Friedel pairs on both +2θ and –2θ)
Range	83–92° 2θ
Temperature	296 K
Diffraction intensity collection	
Radiation	Mo$K\alpha$ (0.71073 Å)
Monochromator	High crystallinity graphite crystal
Range	3–95° 2θ
Reciprocal space range	$0 \le h, k \le 12$ $0 \le l \le 20$
Scan method	ω
Scan range	2.4° 2θ
Scan speed	Variable 2.93–29.30° 2θ/min
Temperature	296 K
Data reduction	
Refinement	SHELXTL-PC
Corrections	Lorentz, Polarization
Absorption correction	Semi-empirical, 13 Ψ scans (10–95° 2θ)

PROCEDURE FOR DETERMINATION OF CATION DISTRIBUTION

As previously discussed, and in close relation with the topochemistry of cubic spinels, in tetragonal manganites A and B cations may be disordered between T and M sites.

Several differing procedures may be adopted to determine cation distribution in minerals, and very satisfactory results have been obtained recently by combining data from single-crystal X-ray structural refinement and electron microprobe analysis (Carbonin et al. 1996; Della Giusta et al. 1996; Lucchesi et al. 1997, 1998a, 1998b, 1999). This procedure reproduces observed parameters by optimizing cation distributions. Differences between observed and calculated parameters are minimized by using the "chi-square" function:

$$F(X_i) = \frac{1}{n} \sum_{j=1}^{n} \left(\frac{O_j - C_j(X_i)}{\sigma_j} \right)^2 \quad (1)$$

TABLE 3. Crystal data and results of crystal structure refinement

Samples	2A	2B	3A	3B	4B	4C	5A	6A	8A	8B
a (Å)	5.7591(4)	5.7584(3)	5.7535(7)	5.7607(5)	5.7554(2)	5.7548(2)	5.7524(4)	5.7625(3)	5.7619(3)	5.7632(2)
c (Å)	9.4464(11)	9.4476(8)	9.4282(15)	9.4601(12)	9.4322(6)	9.4298(6)	9.4078(7)	9.4611(7)	9.4532(6)	9.4547(6)
y	0.4720(2)	0.4724(3)	0.4726(3)	0.4721(3)	0.4729(3)	0.4725(2)	0.4728(3)	0.4721(2)	0.4723(2)	0.4724(2)
z	0.2585(2)	0.2585(2)	0.2586(2)	0.2589(2)	0.2587(2)	0.2584(2)	0.2581(2)	0.2586(1)	0.2588(1)	0.2588(1)
T-O (Å)	2.038(1)	2.037(2)	2.034(2)	2.041(2)	2.033(2)	2.033(1)	2.027(2)	2.040(1)	2.040(1)	2.040(1)
V_T (Å^3)	4.312(3)	4.300(3)	4.280(4)	4.327(3)	4.278(3)	4.277(3)	4.243(4)	4.322(3)	4.319(3)	4.317(3)
$\langle\lambda_T\rangle$	1.0053	1.0055	1.0055	1.0057	1.0057	1.0053	1.0050	1.0055	1.0057	1.0057
O-T-O (°)	103.55	103.45	103.43	103.32	103.32	103.53	103.73	103.45	103.34	103.34
T m.a.n.	24.8(3)	25.1(2)	26.1(4)	24.5(3)	25.6(3)	25.6(3)	26.3(3)	25.2(2)	24.9(2)	25.1(2)
M-O_L (Å)	2.287(1)	2.287(2)	2.281(2)	2.287(2)	2.281(2)	2.284(2)	2.282(2)	2.290(1)	2.285(1)	2.286(1)
M-O_S (Å)	1.927(1)	1.928(1)	1.928(2)	1.928(1)	1.930(1)	1.928(1)	1.928(2)	1.929(1)	1.929(1)	1.930(1)
V_M (Å^3)	11.151(7)	11.170(7)	11.134(8)	11.163(7)	11.158(7)	11.149(7)	11.148(8)	11.185(6)	11.172(5)	11.185(6)
$\langle\lambda_M\rangle$	1.0239	1.0236	1.0232	1.0240	1.0229	1.0233	1.0227	1.0240	1.0236	1.0235
O_S-M-O_L (°)	84.58	84.63	84.62	84.50	84.63	84.68	84.82	84.58	84.53	84.58
O_S-M-O_S (°)	83.11	83.21	83.27	83.14	83.35	83.26	83.34	83.14	83.19	83.21
M m.a.n.	25.1(3)	25.0(2)	24.8(4)	25.1(3)	24.9(3)	24.9(2)	25.0(3)	24.8(2)	25.1(2)	25.0(2)
Ueq. T	67(1)	63(1)	94(1)	56(1)	63(1)	64.3(9)	76(1)	71.6(9)	54.3(7)	73.4(8)
Ueq. M	52.0(7)	50.2(8)	78(1)	43.4(8)	47.8(8)	48.8(8)	63.3(9)	58.0(7)	42.8(6)	59.5(7)
Ueq. O	67(3)	62(3)	94(4)	52(3)	61(3)	61(3)	76(3)	72(3)	53(2)	72(2)
Ext.	0.0010(3)	0.0014(2)	0.0019(4)	0.0011(2)	0.0046(4)	0.0036(3)	0.0024(3)	0.0008(2)	0.0067(4)	0.0040(4)
N > 2σ	411	411	411	411	411	411	411	412	411	411
R	0.0243	0.0210	0.0259	0.0225	0.0236	0.0217	0.0260	0.0201	0.0178	0.0214

Notes: m.a.n. = mean atomic number; Ext. = Isotropic secondary extinction coefficient; R in the form: $(\Sigma|F_{obs} - F_{calc}|)/(\Sigma F_{obs})$; displacement parameters Å$^2 \times 10^4$.

TABLE 4. Electron microprobe analyses

Sample	2A	2B	3A	3B	4B	4C	5A	6A	8A	8B
MnO	89.6(9)	88(3)	89(1)	92.0(7)	87.0(7)	87.0(2)	83.4(5)	92.7(8)	91.7(4)	91.3(9)
MgO	0.4(2)	0.27(8)	0.13(5)	0.52(4)	0.45(5)	0.47(6)	–	0.12(7)	0.03(2)	0.01(1)
ZnO	2.5(6)	3(2)	5.4(4)	0.2(1)	5.3(5)	4.9(5)	9.2(5)	tr.	0.73(4)	0.5(2)
Al_2O_3	–	–	–	–	–	–	tr.	–	0.12(1)	0.08(5)
Total	92.55	91.72	94.07	92.67	92.77	92.41	92.66	92.84	92.61	91.87
MnO*	27.9	27.0	26.2	30.0	25.4	25.6	22.5	30.8	30.2	30.1
Mn_2O_3*	68.7	67.8	69.3	69.0	68.6	68.4	67.9	68.9	68.5	68.0
	Formula proportions based on 3 cations and 4 oxygen atoms									
Mg	0.03(1)	0.015(6)	0.007(5)	0.029(3)	0.026(4)	0.027(4)	–	0.007(5)	0.002(1)	0.001(1)
Mn^{2+}	0.90(4)	0.89(9)	0.84(3)	0.97(1)	0.83(3)	0.83(3)	0.74(2)	0.99(1)	0.978(7)	0.98(2)
Zn	0.07(2)	0.10(7)	0.15(2)	0.005(4)	0.15(2)	0.14(2)	0.26(2)	0.000	0.021(2)	0.015(9)
Al	–	–	–	–	–	–	0.000	–	0.005(1)	0.004(3)
Mn^{3+}	2.00(3)	2.00(8)	2.00(2)	2.000(8)	2.00(2)	2.00(2)	2.00(2)	2.000(9)	1.995(5)	2.00(1)

Notes: No less than 15 point analyses for each sample.
* Calculated from stoichiometry.

where O_j is the observed quantity, σ_j its standard deviation, X_i are variables, i.e., cation fractions in T and M sites, and $C_j(X_i)$ is the same quantity as O_j calculated by means of X_i parameters. The n O_j quantities taken into account were: unit-cell and oxygen parameters *a*, *c*, *y*, *z*, mean atomic number (m.a.n.) of T and M sites, and total atomic proportions from microprobe analyses. Minimization of equation 1, up to convergence, was performed using the MINUIT program (James and Roos 1975) linked to a home-developed calculation routine; further details about the minimization procedure may be found in Lucchesi et al. (1999) and Lavina et al. (2002). In the case of spinel and hausmannite structures, unit-cell parameters and oxygen coordinates are functions of bond angles and bond lengths, and the latter may be calculated, within the framework of the ionic model (Burnham 1990), as the linear contribution of each site cation population multiplied by its specific site bond distance.

Application of this calculation to hausmannite is not straightforward, since both T and M sites are remarkably distorted, resulting in variations in bond-distance dimensions. To overcome this difficulty, the above-described method was applied to polyhedral volumes assuming that, for the same site population, the numerical values of volumes of regular and distorted polyhedra are equal. Concerning the tetrahedron, combining its polyhedral volume V_T (see Appendix Table 1) with its regular equivalent $\left[V_{T_r} = (T-O)_r^3 \frac{8}{9\sqrt{3}}\right]$ yields:

$$\frac{(T-O)_r^3}{(T-O)^3} = \frac{3\sqrt{3}}{2}\cos\left(\frac{\Phi}{2}\right)\sin^2\left(\frac{\Phi}{2}\right) \quad (2)$$

from which it turns out that T-O is always larger than T-O_r: the bond distance of a given cation in hausmannite is expected to be larger than the corresponding one for cubic spinels. For instance, the $^{IV}Mn^{2+}$-O bond distance is 2.036 Å in cubic spinels (Lucchesi et al. 1997) and may be calculated (Eq. 2) as 2.041 Å for hausmannite with ϕ = 103.5° (e.g., sample 6A, Table 3). The effect of distortion on polyhedral geometry is particularly evident for $^{VI}Mn^{3+}$ because, in this case, the octahedron is distorted not only in terms of bond angles but also shows large differences in cation-to-oxygen distances. Inspection of octahedral dimensions obtained from structural data of $^{VI}Mn^{3+}$-rich crystals (Shannon et al. 1975), indicates that octahedral dimensions increase with polyhedral distortion, so that $^{VI}Mn^{3+}$ ionic radius (ranging between 0.62 and 0.67Å) cannot be considered representative for all Mn^{3+} octahedra in all structures. The difficulty in calculating the contributions of site populations to M-O_L and M-O_S bond distances suggested applying the same method used for tetrahedra.

The numerical values of volumes of hausmannite polyhedra (V_T and V_M) and regular polyhedra (V_{Tr} and V_{Mr}) were thus assumed as equal in the case of the same site population, according to the following equations:

$$V_T = V_{Tr} = \frac{8}{9\sqrt{3}}\left[\sum X_i (\mathrm{T-O})_{ir}\right]^3$$

$$V_M = V_{Mr} = \frac{4}{3}\left[\sum X_i (\mathrm{M-O})_{ir}\right]^3$$

where T-O_{ir} and M-O_{ir} are the specific cation-to-oxygen bond distances in spinel structure (Lavina et al. 2002), with M-O_{ir} corrected for distortion of spinel structure, and X_i the T and M site populations. Cell parameters and oxygen fractional coordinates were calculated as functions of T-O, V_T and V_M (Appendix Table 2), in which the O-T-O, M-O_S and M-O_L values used are the observed ones.

During minimization runs, the following assumptions were made: Mn^{2+} and Mn^{3+} were allowed to occupy both M and T sites; on the basis of their general preference, the small amounts of Al were assigned to M site, and Mg and Zn to T site. A specific bond distance of 2.030 Å was adopted for $^{VI}Mn^{3+}$, since it gave the best fit for the examined samples; that for $^{IV}Mn^{3+}$ (1.889 Å) was calculated on the basis of the mean difference reported by Shannon (1976) for transition elements in fourfold and sixfold coordination.

Results

The samples belong to the hausmannite-hetaerolite series ($MnMn_2O_4$-$ZnMn_2O_4$), since the main substitution among bivalent cations involves $Mn^{2+} \leftrightarrow Zn$, and Mn^{3+} is almost constant and stoichiometric in all samples (Table 4). In particular, Mn^{2+} ranges from 0.739 to 0.993 atoms per formula unit (apfu) and Zn reaches its highest concentration (0.263 apfu) in sample 5A. The only other bivalent cation is Mg, which, however, only occurs in very small concentrations (not exceeding 0.029 apfu). Among trivalent cations, Mn^{3+} is by far the most abundant (1.994–2.000 apfu), with only very minor quantities of Al (up to 0.005 apfu) in samples 8A and 8B, which come from Ilfeld. No Fe was detected.

The intersite cation distribution of each sample is shown in Table 5, in which a good fit between observed and calculated structural parameters is clear. Differences between observed and calculated values were always within the limits of experimental error. Considering that the number of free parameters (X_i) in Equation 1 ranged from 3 to 5, final values of F(X_i) < 1 represent very good modeling of experimental data. The very small or nil amounts of $^{VI}Mn^{2+}$ and $^{IV}Mn^{3+}$ are clear evidence of the highly normal distribution of Mn.

Unit-cell parameters a and c range from 5.7524 to 5.7632 Å and from 9.4078 to 9.4611 Å, respectively. Negative linear relations may be observed between Zn content and unit-cell parameters:

a = 5.7622 – 0.0436 Zn (R^2 = 0.90)
c = 9.4601 – 0.1967 Zn (R^2 = 0.97).

An increase in Zn causes a decrease in the c/a ratio (ranging from 1.642 in samples 6A and 3B to 1.636 in sample 5A), resulting in progressive closing to cubic symmetry (in which c/a = 1.414).

Concerning the tetrahedron, variable parameters are T-O

Table 5. Cation distribution, calculated and observed structural parameters and minimisation residuals F(X_i)

Sample	2A	2B	3A	3B	4B	4C	5A	6A	8A	8B
Site T										
Mg	0.024	0.014	0.006	0.029	0.025	0.025	–	0.005	0.002	0.001
Zn	0.049	0.062	0.147	0.005	0.132	0.121	0.244	–	0.021	0.018
Mn^{2+}	0.928	0.924	0.848	0.966	0.845	0.854	0.758	0.994	0.977	0.981
Mn^{3+}	0.000	0.000	0.000	0.000	0.000	0.001	0.000	0.000	0.000	0.000
Total	1.001	1.000	1.001	1.001	1.002	1.001	1.002	1.000	1.000	1.000
Site M										
Mn^{2+}	0.002	0.003	0.000	0.003	0.003	0.000	0.003	0.004	0.003	0.004
Mn^{3+}	1.998	1.998	1.999	1.998	1.997	2.000	1.997	1.998	1.994	1.995
Al	–	–	–	–	–	–	–	–	0.005	0.003
Total	2.000	2.001	1.999	2.000	2.000	2.000	2.000	2.001	2.001	2.002
$a_{obs.}$	5.7591(4)	5.7584(3)	5.7535(8)	5.7607(5)	5.7554(2)	5.7548(2)	5.7524(4)	5.7625(3)	5.7619(3)	5.7632(2)
$a_{calc.}$	5.7589	5.7584	5.7530	5.7606	5.7553	5.7547	5.7520	5.7626	5.7619	5.7633
$c_{obs.}$	9.4464(11)	9.4476(8)	9.4282(15)	9.4601(12)	9.4322(6)	9.4298(6)	9.4078(7)	9.4611(7)	9.4532(6)	9.4547(6)
$c_{calc.}$	9.4467	9.4475	9.4291	9.4602	9.4324	9.4300	9.4081	9.4608	9.4531	9.4545
$y_{obs.}$	0.4720(2)	0.4724(3)	0.4726(3)	0.4721(3)	0.4729(3)	0.4725(2)	0.4728(3)	0.4721(2)	0.4723(2)	0.4724(2)
$y_{calc.}$	0.4720	0.4724	0.4728	0.4721	0.4729	0.4726	0.4729	0.4720	0.4723	0.4724
$z_{obs.}$	0.2585(2)	0.2585(2)	0.2586(2)	0.2589(2)	0.2587(2)	0.2584(2)	0.2581(2)	0.2586(1)	0.2588(1)	0.2588(1)
$z_{calc.}$	0.2585	0.2585	0.2585	0.2588	0.2587	0.2584	0.2580	0.2586	0.2588	0.2588
T m.a.n.$_{obs.}$	24.8(3)	25.1(2)	26.1(4)	24.5(3)	25.6(3)	25.6(3)	26.3(3)	25.2(2)	24.9(2)	25.1(2)
T m.a.n.$_{calc.}$	24.9	25.1	25.7	24.7	25.4	25.3	26.3	24.9	25.1	25.1
M m.a.n.$_{obs.}$	25.1(3)	25.0(2)	24.8(4)	25.1(3)	24.9(3)	24.9(2)	25.0(3)	24.8(2)	25.1(2)	25.0(2)
M m.a.n.$_{calc.}$	25.0	25.0	25.0	25.0	25.0	25.0	25.0	25.0	25.0	25.0
F(X_i)	0.39	0.16	0.51	0.17	0.58	0.59	0.91	0.78	0.31	0.47

Notes: obs. = observed; calc.= calculated; m.a.n.= mean atomic number.

bond distance (2.027–2.041 Å) and the O-T-O angle (103.3–103.7°). They are not interrelated, but T-O shows strong positive correlations with *a* (Fig. 1a, $R^2 = 0.86$), *c* (Fig. 1b, $R^2 = 0.97$), and *c/a* ($R^2 = 0.94$). Instead, $\langle\lambda_T\rangle$ (Robinson et al. 1971) and consequently O-T-O (see Appendix) are significantly related only to oxygen coordinate *z* ($R^2 = 0.94$).

Of the two non-equivalent octahedral bond distances, M-O_L and M-O_S, the latter shows a very small variation, from 1.927 to 1.930 Å. The longer distance, M-O_L, shows a larger variation, from 2.281 to 2.290 Å, and is positively correlated with *c* (Fig. 2, $R^2 = 0.74$). Distortion of the octahedron, $\langle\lambda_M\rangle$ (Robinson et al. 1971) ranges from 1.0227 to 1.0240, and its decrease coincides with an increase in *y* ($R^2 = 0.94$) and decrease in *c* ($R^2 = 0.81$) and *c/a* ($R^2 = 0.83$).

DISCUSSION AND CONCLUSIONS

The crystals examined in this study are characterized by almost homogeneous composition in terms of trivalent cations, so that all the observed structural distortions are restricted to the effects of divalent cations. Given the highly normal cation distribution, the geometry of T site closely depends on $^{IV}Zn \leftrightarrow {}^{IV}Mn^{2+}$ substitution. This is evident from the linear relation between Zn and T-O bond distance ($R^2 = 0.98$; Fig. 3). The smaller bond distance of ^{IV}Zn-O (1.960 Å) with respect to $^{IV}Mn^{2+}$-O (2.036 Å) explains tetrahedral contraction during $^{IV}Zn \rightarrow {}^{IV}Mn^{2+}$ substitution.

As the octahedral content of all samples is almost identical, given the closeness of $^{VI}Mn^{3+}$ to stoichiometry (1.993–2.000 apfu), all octahedral distortions are not due to variations in its composition but to the "dragging effect" of the tetrahedron on the octahedron. This feature is evident not only from the geometrical relation concerning V_M (see Appendix), but also the positive relations between $\langle\lambda_M\rangle$ and V_T values ($R^2 = 0.84$; Fig. 4). Moreover, octahedral distortion closely depends on M-O_L values ($R^2 = 0.83$) rather than M-O_S ones, and M-O_L variations, in turn, are due to dimensional variations in the tetrahedron. In fact, $^{IV}Zn \rightarrow {}^{IV}Mn^{2+}$ substitution produces not only contraction of the T-O bond distance but also shortening of the M-O_L bond distance ($R^2 = 0.72$).

In summary, Zn content has a large negative effect on unit-cell parameters, particularly *c* and the *c/a* ratio, resulting in progressive movement of the structure toward cubic symme-

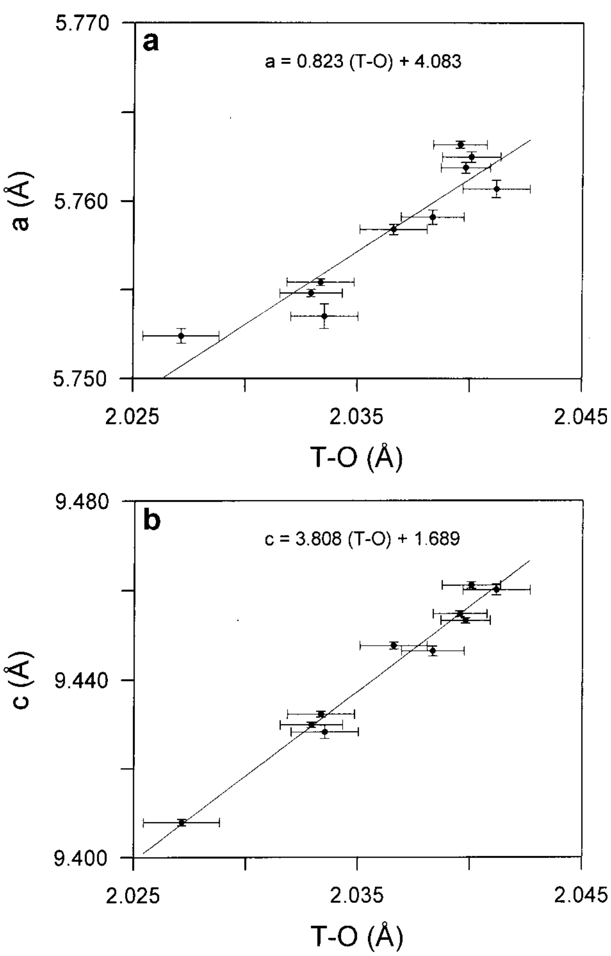

FIGURE 1. Plots of (**a**) *a* vs. T-O and (**b**) *c* vs. T-O in hausmannite.

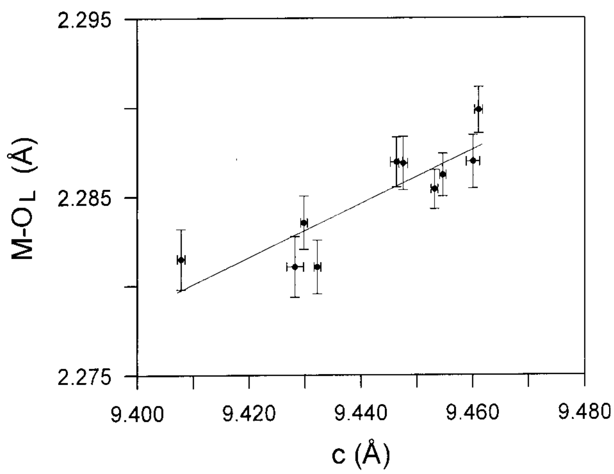

FIGURE 2. Plot of M-O_L vs. *c* in hausmannite.

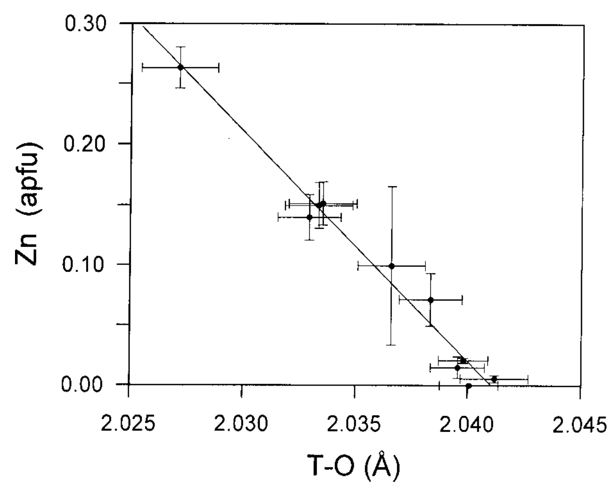

FIGURE 3. Plot of Zn vs. T-O in hausmannite.

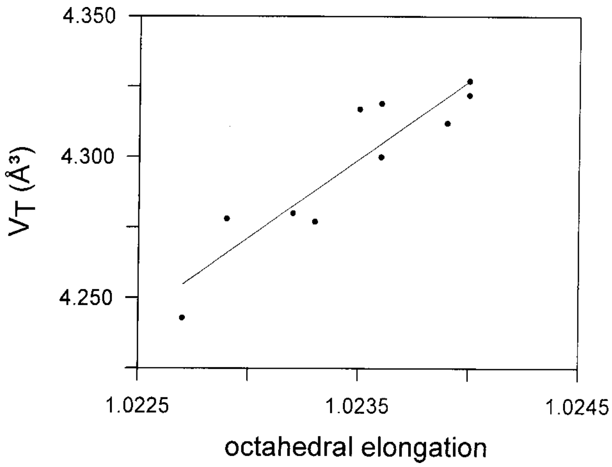

FIGURE 4. Plot of V_T vs. octahedral elongation in hausmannite.

try. These effects also involve oxygen, which moves toward values characteristic of cubic spinels, with the oxygen coordinate z related to $<\lambda_T>$ and y to $<\lambda_M>$.

In hausmannite-type structures, besides the main structural distortion produced by the Jahn-Teller effect, a secondary one, without any changes in symmetry, is caused by the geometrical effects of the tetrahedron on the octahedron. Tetrahedral volume and distortion depend only on T-site cations, whereas volume and distortion of M-site depend on the features of both T and M sites (see Appendix, Table 2). The "regularization" of the octahedron is thus due to a "dragging effect" that leads toward cubic symmetry with increasing hetaerolite contents.

ACKNOWLEDGMENTS

The authors express their gratitude to the "Museo di Mineralogia" of the University of Rome "La Sapienza" for furnishing samples. R. Carampin carried out electron microprobe analyses. Gabriel Walton revised the English text. This work was funded by CNR and MURST grants and carried out within scientific programs and with the financial support of the C.S.–CNR "Equilibri sperimentali in minerali e rocce."

REFERENCES CITED

Burnham, C.W. (1990) The ionic model: Perceptions and realities in mineralogy. American Mineralogist, 75, 443–463.

Carbonin, S., Russo, U., and Della Giusta, A. (1996) Cation distribution in some natural spinels from X-ray diffraction and Mössbauer spectroscopy. Mineralogical Magazine, 60, 355–368.

Della Giusta, A., Carbonin, S., and Ottonello, G. (1996) Temperature-dependent disorder in a natural Mg-Al-Fe^{2+}-Fe^{3+}-spinel. Mineralogical Magazine, 60, 603–616.

Golikov, Y.V., Barkhatov, V.P., Balakirev, V.F., and Avdukov, V.I. (1989) High-temperature and quenched states in manganese-containing oxide systems in air. High Temperatures-High Pressures, 21, 685–700.

Hafner, S. (1960) Metalloxyde mit Spinellstruktur. Schweizerische Mineralogische und Petrographische Mitteilungen, 40, 208–240.

Hill, R.J., Craig, J.R., and Gibbs, G.V. (1979) Systematics of the spinel structure type. Physics and Chemistry of Minerals, 4, 317–339.

James, F. and Roos, M. (1975) MINUIT, a system for function minimization and analysis of the parameters errors and correlations. Computer Physics Communications, 10, 343–367.

Jarosch, D. (1987) Crystal Structure Refinement and Reflectance Measurements of Hausmannite, Mn_3O_4. Mineralogy and Petrology, 37, 15–23.

Lavina, B., Salviulo, G., and Della Giusta, A. (2002) Cation distribution and structure modelling of spinel solid solutions. Physics and Chemistry of Minerals, 29, 10–18.

Lucchesi, S., Russo, U., and Della Giusta, A. (1997) Crystal chemistry and cation distribution in some Mn-rich natural and synthetic spinels. European Journal of Mineralogy, 9, 31–42.

Lucchesi, S., Della Giusta, A., and Russo, U. (1998a) Cation distribution in natural Zn-aluminate spinels. Mineralogical Magazine, 62, 41–54.

Lucchesi, S., Amoriello, M., and Della Giusta, A. (1998b) Crystal chemistry of spinels from xenoliths of the Alban Hills volcanic region. European Journal of Mineralogy, 10, 473–482.

Lucchesi, S., Russo, U., and Della Giusta, A. (1999) Cation distribution in natural Zn-spinels: franklinite. European Journal of Mineralogy, 11, 501–511.

Robinson, K., Gibbs, G.V., and Ribbe, P.H. (1971) Quadratic elongation: A quantitative measure of distortion in coordination polyhedra. Science, 172, 567–570.

Satomi, K. (1961) Oxygen positional parameters of tetragonal Mn_3O_4. Journal of the Physical Society of Japan, 16, 258–266.

Shannon, R.D. (1976) Revised effective ionic radii and systematic studies of interatomic distances in halides and chalcogenides. Acta Crystallographica, A32, 751–767.

Shannon, R.D., Gumerman, P.S., and Chenavas, J. (1975) Effect of octahedral distortion on mean Mn^{3+}-O distances. American Mineralogist, 60, 714–716.

MANUSCRIPT RECEIVED JUNE 18, 2001
MANUSCRIPT ACCEPTED MARCH 10, 2002
MANUSCRIPT HANDLED BY JEFFREY E. POST

APPENDIX: GEOMETRICAL RELATIONS BETWEEN CUBIC AND TETRAGONAL MULTIPLE OXYDES

Interatomic distances and angles may be calculated for $I4_1/amd$ hausmannite tetragonal structure (Appendix Table 1) in terms of unit-cell parameters (a, c) and oxygen positional coordinates (0, y, z). Lattice parameters and oxygen coordinates (Appendix, Table 2) may, in turn, be expressed in terms of bond distances T-O, M-O_L, M-O_S and tetrahedral angle O-T-O (thereafter ϕ).

APPENDIX TABLE 1. Interatomic distances, site volumes, and Robinson's elongations in tetragonal manganites

Site T	Site M
$\mathrm{T-O} = \sqrt{\left(\frac{3}{4}-y\right)^2 a^2 + \left(z-\frac{1}{8}\right)^2 c^2}$	$\mathrm{M-O_L} = \sqrt{\left(y-\frac{1}{2}\right)^2 a^2 + \left(z-\frac{1}{2}\right)^2 c^2}$
$(\mathrm{T-O})\cos\left(\frac{\phi}{2}\right) = c\left(z-\frac{1}{8}\right)$	$\mathrm{M-O_S} = \sqrt{\left(y^2-\frac{1}{2}y+\frac{1}{8}\right)a^2 + \left(z-\frac{1}{8}\right)^2 c^2}$
$V_T = \frac{4}{3}(\mathrm{T-O})^3\cos\left(\frac{\phi}{2}\right)\sin^2\left(\frac{\phi}{2}\right)$	$V_M = \frac{1}{12}a^2c - \frac{2}{3}a(\mathrm{T-O})^2\sin(\phi) - \frac{1}{3}(\mathrm{T-O})^2 c\sin^2\left(\frac{\phi}{2}\right) + 2V_T$
$\langle\lambda_T\rangle = \left[\frac{3\sqrt{3}}{2}\cos\left(\frac{\phi}{2}\right)\sin^2\left(\frac{\phi}{2}\right)\right]^{-2/3} = \left(\frac{V_T}{V_{Tr}}\right)^{-2/3}$	$<\lambda_M> = \frac{(\mathrm{M-O})_L^2 + (\mathrm{M-O})_S^2}{3\left(\frac{9}{16}V_M^2\right)^{1/3}}$

APPENDIX TABLE 2. Lattice parameters and oxygen coordinates as functions of bond distances (T-O, M-O$_L$, M-O$_s$) and angle (ϕ)

$$c = -\frac{4}{11}\left(\frac{-C\sqrt{B} + 37\,(T\text{-}O)^2 - 47\,(T\text{-}O)^2\cos^2(\phi/2) - 110\,(M\text{-}O)_L^2 + 22\,(M\text{-}O)_S^2 - A}{\sqrt{6\,C\sqrt{B} - 222\,(T\text{-}O)^2 + 282\,(T\text{-}O)^2\cos^2(\phi/2) + 660\,(M\text{-}O)_L^2 - 132\,(M\text{-}O)_S^2}} - 7\,(T\text{-}O)\cos(\phi/2)\right)$$

$$\begin{aligned} A = \{ & (M\text{-}O)_S^4[968 - 1936\,C^2] + (M-O)_L^4[24200 - 48400\,C^2] + (T\text{-}O)^4[2738 - 7177\,C^2] + \\ & + (M-O)_S^2\,(T\text{-}O)^2[3256 + 4180\,C^2] - (M-O)_L^2\,(T\text{-}O)^2[16280 - 31372\,C^2] - (M-O)_L^2\,(M-O)_S^2\,[9680 - 19360\,C^2] + \\ & + (T\text{-}O)^2\cos^2(\phi/2)\,[\,20680\,(M-O)_L^2 - 4136\,(M-O)_S^2 - 6956\,(T\text{-}O)^2 - 40172\,C^2\,(M-O)_L^2 - 2420\,C^2\,(M-O)_S^2 + \\ & + 47\,C\sqrt{B} + 12346\,C^2\,(T\text{-}O)^2\,] + 110\,C\sqrt{B}\,(M-O)_L^2 + \\ & + 81\,(T\text{-}O)^3\cos(\phi/2)\sin^2(\phi/2)\sqrt{6\,C\sqrt{B} - 222\,(T\text{-}O)^2 + 282\,(T\text{-}O)^2\cos^2(\phi/2) + 660\,(M\text{-}O)_L^2 - 132\,(M\text{-}O)_S^2} + \\ & + (T\text{-}O)^4\cos^4(\phi/2)\,[4418 - 5569\,C^2] - 37\,C\sqrt{B}\,(T\text{-}O)^2 - 22\,C\sqrt{B}\,(M-O)_S^2\,\}^{1/2} \end{aligned}$$

$$\begin{aligned} B = \; & 1936\,(M\text{-}O)_S^4 - 4180\,(M\text{-}O)_S^2\,(T\text{-}O)^2 - 19360\,(M\text{-}O)_L^2\,(M\text{-}O)_S^2 - 31372\,(M\text{-}O)_L^2\,(T\text{-}O)^2 + 48400\,(M\text{-}O)_L^4 + 7177\,(T\text{-}O)^4 + \\ & + (T\text{-}O)^2\cos^2(\phi/2)\,[2420\,(M\text{-}O)_S^2 - 12346\,(T\text{-}O)^2 + 40172\,(M\text{-}O)_L^2] + 5569\,(T\text{-}O)^4\cos^4(\phi/2) \end{aligned}$$

$$C = \cos\left[\frac{1}{3}\arccos\left(-\frac{D}{\sqrt{B^3}}\right)\right]$$

$$D = \left(\begin{aligned} & 594035\,(T\text{-}O)^6 - 409303\,(T\text{-}O)^6\cos^6(\phi/2) - 10648000\,(M\text{-}O)_L^6 + 85184\,(M\text{-}O)_S^6 \\ & -4043622\,(T\text{-}O)^4\,(M\text{-}O)_L^2 + 10352760\,(M\text{-}O)_L^4\,(T\text{-}O)^2 - 275880\,(M\text{-}O)_S^4\,(T\text{-}O)^2 \\ & +\cos^2(\phi/2)[\,-1649613\,(T\text{-}O)^6 - 13256760\,(M\text{-}O)_L^4\,(T\text{-}O)^2 + 159720\,(M\text{-}O)_S^4\,(T\text{-}O)^2 + 8365764\,(T\text{-}O)^4\,(M\text{-}O)_L^2 \\ & +961356\,(T\text{-}O)^4\,(M\text{-}O)_S^2 + 1852752\,(M\text{-}O)_L^2\,(M\text{-}O)_S^2\,(T\text{-}O)^2\,] \\ & +\cos^4(\phi/2)\,[\,1456881\,(T\text{-}O)^6 - 556842\,(M\text{-}O)_S^2\,(T\text{-}O)^4 - 4586142\,(T\text{-}O)^4\,(M\text{-}O)_L^2\,] \\ & -1277760\,(M\text{-}O)_S^4\,(M\text{-}O)_L^2 - 351714\,(M\text{-}O)_S^2\,(T\text{-}O)^4 + 6388800\,(M\text{-}O)_S^2\,(M\text{-}O)_L^4 - 691152\,(M\text{-}O)_S^2\,(M\text{-}O)_L^2\,(T\text{-}O)^2 \end{aligned}\right)$$

$$a = \frac{8}{5}\,(T\text{-}O)\sin(\phi/2) + \frac{1}{10}\sqrt{-64\,(T\text{-}O)^2 - 256\,(T\text{-}O)^2\cos^2(\phi/2) + 320\,(M\text{-}O)_S^2 + 80\,c\,(T\text{-}O)\cos(\phi/2) - 5\,c^2}$$

$$y = \frac{3}{4} - \frac{(T-O)\sin(\phi/2)}{a}$$

$$z = \frac{1}{8} + \frac{(T-O)\cos(\phi/2)}{c}$$

Note: Only the relation concerning *c* is totally explicated, whereas the others, for the sake of brevity, are reported in terms of unit-cell parameters, so that they must be developed in sequence.